

# Forward and Backward Bifurcation Analysis From an Imperfect Vaccine Efficacy Model with Saturated Treatment and Saturated Infection

Hakan Ahmad Fatahillah and Dipo Aldila



Volume 5, Issue 2, Pages 132–143, December 2024

Received 10 December 2024, Revised 27 January 2025, Accepted 29 January 2025, Published Online 30 January 2025

To Cite this Article : H. A. Fatahillah and D. Aldila, "Forward and Backward Bifurcation Analysis From an Imperfect Vaccine Efficacy Model with Saturated Treatment and Saturated Infection", *Jambura J. Biomath*, vol. 5, no. 2, pp. 132–143, 2024, <https://doi.org/10.37905/jjbm.v5i2.28810>

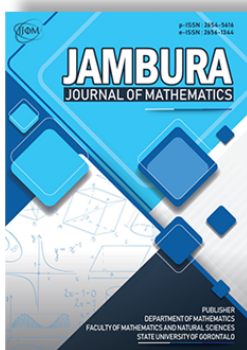
© 2024 by author(s)

## JOURNAL INFO • JAMBURA JOURNAL OF BIOMATHEMATICS



	Homepage	:	<a href="http://ejournal.ung.ac.id/index.php/JJBM/index">http://ejournal.ung.ac.id/index.php/JJBM/index</a>
	Journal Abbreviation	:	Jambura J. Biomath.
	Frequency	:	Biannual (June and December)
	Publication Language	:	English
	DOI	:	<a href="https://doi.org/10.37905/jjbm">https://doi.org/10.37905/jjbm</a>
	Online ISSN	:	2723-0317
	Editor-in-Chief	:	Hasan S. Panigoro
	Publisher	:	Department of Mathematics, Universitas Negeri Gorontalo
	Country	:	Indonesia
	OAI Address	:	<a href="http://ejournal.ung.ac.id/index.php/jjbm/oai">http://ejournal.ung.ac.id/index.php/jjbm/oai</a>
	Google Scholar ID	:	XzYgeKQAAAAJ
	Email	:	<a href="mailto:editorial.jjbm@ung.ac.id">editorial.jjbm@ung.ac.id</a>

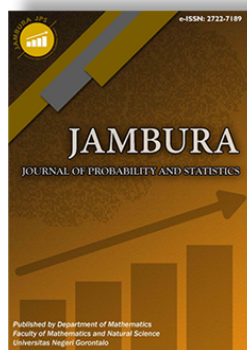
## JAMBURA JOURNAL • FIND OUR OTHER JOURNALS



Jambura Journal of Mathematics



Jambura Journal of Mathematics Education



Jambura Journal of Probability and Statistics



EULER : Jurnal Ilmiah Matematika, Sains, dan Teknologi

# Forward and Backward Bifurcation Analysis From an Imperfect Vaccine Efficacy Model with Saturated Treatment and Saturated Infection

Hakan Ahmad Fatahillah<sup>1</sup> and Dipo Aldila<sup>1,\*</sup> 

<sup>1</sup>Department of Mathematics, Faculty of Mathematics and Natural Sciences, Universitas Indonesia, Depok 16424, Indonesia.

## ARTICLE HISTORY

Received 10 December 2024  
Revised 27 January 2025  
Accepted 29 January 2025  
Published 30 January 2025

## KEYWORDS

Vaccination  
Imperfect Efficacy  
Bifurcation  
Basic Reproduction Number

**ABSTRACT.** This paper aims to study the saturation effect on the infection and recovery process within a Susceptible-Vaccination-Infected model featuring an imperfect vaccine efficacy. First, we nondimensionalized the model under the assumption of a constant population, resulting in the reduction of the model from three to two-dimensional differential equations. The analysis indicates the presence of a disease-free equilibrium (DFE) and potentially multiple endemic equilibria (EE) within the model. The calculation of the basic reproduction number further explains the model's solution conditions. In particular, we discovered that a backward bifurcation is possible under specific saturation effect values. Dulac's criterion confirmed the absence of a closed orbit in the solution region, suggesting the global stability of the endemic equilibrium when the basic reproduction number exceeds one. To supplement the analytical study, a numerical simulation was conducted to generate a bifurcation diagram, autonomous simulation, and global sensitivity analysis. The global sensitivity analysis revealed that changing the vaccination rate or recovery rate could significantly impact the basic reproduction number. Moreover, the bifurcation diagram depicting the relationship between the transmission rate and vaccination rate demonstrated that increasing the vaccination rate while maintaining the transmission rate can reduce the proportion of infected individuals within the population.



This article is an open access article distributed under the terms and conditions of the Creative Commons Attribution-NonCommercial 4.0 International License. *Editorial of JJBM:* Department of Mathematics, Universitas Negeri Gorontalo, Jln. Prof. Dr. Ing. B. J. Habibie, Bone Bolango 96554, Indonesia.

## 1. Introduction

Mathematical models have been extensively utilized by researchers to understand the spread of diseases within populations, such as dengue [1–5], malaria [6–10], COVID-19 [11–16], Tuberculosis (TB) [17–24], the recent Mpox [25–29], and many other diseases [30–35]. The objectives of these models range from elucidating the mechanisms of disease transmission to projecting future scenarios based on the types of intervention required. A common feature these models share is the use of the basic reproduction number, denoted as  $\mathcal{R}_0$ , as an endemic indicator. Generally, the findings indicate that a disease will persist in the population if the basic reproduction number exceeds one, while it may be eradicated if  $\mathcal{R}_0$  is less than one [36].

The condition of disease persistence, characterized by a reproduction number greater than one, is consistently observed in the literature. However, the disappearance of the disease when the basic reproduction number is less than one is always guaranteed. This scenario may arise if a backward bifurcation occurs when the basic reproduction number equals one. In such cases, a stable disease-free equilibrium (DFE) coexists with a stable endemic equilibrium even when the basic reproduction number is less than one [37]. Consequently, reducing the basic reproduction number below one may not always lead to disease elimination. The emergence of backward bifurcation can be attributed

to various factors, such as reinfection, relapse, treatment failure in tuberculosis transmission [23, 38], disease-induced mortality [39], saturated treatment rate [12], saturated transmission rate [40], and other sources. In contrast, forward bifurcation phenomena are easier to interpret biologically. In cases of forward bifurcation, when the basic reproduction number is less than one, the DFE is always stable, and no other equilibrium exists. However, when the basic reproduction number reaches one, the DFE shifts from stable to unstable, and an endemic equilibrium begins to emerge [37].

As mentioned in the previous paragraph, existence of backward bifurcation may trigger a misunderstanding condition of diseases extinction when the basic reproduction number is less than one. Hence, it is important to conduct an analysis on the source of possible backward bifurcation which may appears from several diseases, such as saturated treatment and infection which may appears on a diseases that trigger changes of human behaviour when the outbreak appears. This research examines an additional potential source of backward bifurcation: the saturation effects in treatment and infection rates within an imperfect vaccination model. The model encompasses three compartments: susceptible, vaccinated, and infected populations, integrating saturation effects in transmission and recovery rates. The vaccination is presumed to be flawed, and individuals who have recovered are considered to revert to the susceptible group. The paper is organized in the following format: **Section 2** delineates

\*Corresponding Author.

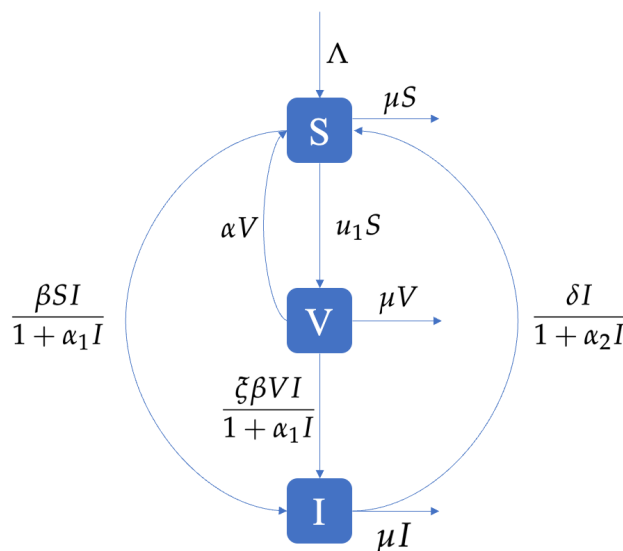


Figure 1. Transmission diagram of the SVI model in (1).

the model construction, whereas Section 3 examines the model analysis, emphasising existence, stability, and bifurcation types. Section 4 subsequently presents numerical simulations which explain the bifurcation diagram and conduct a global sensitivity analysis of  $\mathcal{R}_0$ . In the end, Section 5 finishes the paper with the summary of findings.

### 2. Model Construction

The model consists of three compartments: susceptible population  $S$ , vaccinated population  $V$ , and infected population  $I$ . It incorporates demographic processes such as birth and natural death. Model construction is given as follows and based on transmission diagram depicted in Figure 1. Newborns enter the susceptible compartment at a rate of  $\Lambda$ , and the individuals in each compartment experience natural mortality at a rate of  $\mu$ . We assume that the total population remains constant over time, represented by  $N = S + V + I$ . When a susceptible person joins the vaccination program, they enter the vaccinated compartment at a rate of  $u_1$ . However, due to vaccine imperfections, the vaccinated individual may revert to being susceptible at a rate of  $\alpha$  and could be infected by a reduction of  $\xi$ . Both susceptible and vaccinated individuals could be infected at a rate of  $\beta$ , and infected individuals would recover but remain susceptible to the disease at a rate of  $\delta$ . The transmission and recovery processes undergo saturation at rates of  $\alpha_1$  and  $\alpha_2$ , respectively, depending on the number of infected individuals. This implies that both the transmission and recovery rates will decrease as the number of infected individuals increases. The mathematical model of the spread of the disease with regard to vaccination and saturation is presented by model (1).

$$\begin{aligned}
 \frac{dS}{dt} &= \Lambda - u_1S + \alpha V - \frac{\beta SI}{1 + \alpha_1 I} + \frac{\delta I}{1 + \alpha_2 I} - \mu S, \\
 \frac{dV}{dt} &= u_1S - \alpha V - \frac{\xi \beta VI}{1 + \alpha_1 I} - \mu V, \\
 \frac{dI}{dt} &= \frac{\beta SI}{1 + \alpha_1 I} + \frac{\xi \beta VI}{1 + \alpha_1 I} - \frac{\delta I}{1 + \alpha_2 I} - \mu I,
 \end{aligned}
 \tag{1}$$

with  $S(0) \geq 0, V(0) \geq 0, I(0) \geq 0$ .

Note that all parameters in the model are positive. It is essential to ensure that the solution of this model is nonnegative and bounded. In the boundary region of  $\mathbb{R}_{\geq 0}^3$ , we have

$$\begin{aligned}
 \frac{dS}{dt} \Big|_{S=0, V \geq 0, I \geq 0} &= \Lambda + \alpha V + \frac{\delta I}{1 + \alpha_2 I} \geq 0, \\
 \frac{dV}{dt} \Big|_{S \geq 0, V=0, I \geq 0} &= u_1S \geq 0, \\
 \frac{dI}{dt} \Big|_{S \geq 0, V \geq 0, I=0} &= 0.
 \end{aligned}$$

This computation confirms that initiating the system in the boundary plane indicates that the rates are nonnegative. Thus, setting the initial conditions to be nonnegative ensures that the solution remains nonnegative.

**Theorem 1.** *The solution of model (1) remains nonnegative for all  $t > 0$ , given the nonnegative initial condition.*

Next, since  $N = S + V + I$ , we have  $\frac{dN}{dt} = \frac{dS}{dt} + \frac{dV}{dt} + \frac{dI}{dt} = \Lambda - \mu N$ . Solving this equation for  $N$ , we have  $N = \frac{\Lambda}{\mu} + \frac{N(0)}{e^{\mu t}}$ . When  $t \rightarrow \infty$ , we have  $N \rightarrow \frac{\Lambda}{\mu}$ . Additionally, the solution  $N$  depends on the initial condition  $N(0)$ . We analyze  $\frac{dN}{dt}$  qualitatively. The equilibrium of  $\frac{dN}{dt}$  is  $N = \frac{\Lambda}{\mu}$ . Note that  $\frac{dN}{dt}$  is a linear, monotonically decreasing function over  $N$ . If we let  $N(0) > \frac{\Lambda}{\mu}$ , then  $\frac{dN}{dt} < 0$ . Thus, the solution monotonically decreases to  $\frac{\Lambda}{\mu}$ . Conversely, if we let  $N(0) < \frac{\Lambda}{\mu}$ , then  $\frac{dN}{dt} > 0$  and the solution monotonically increases to  $\frac{\Lambda}{\mu}$ . Therefore, the solution is bounded above by either  $\frac{\Lambda}{\mu}$  or the initial condition. We conclude the results in the next theorem.

**Theorem 2.** *The solution of model (1) is bounded in the region  $\Omega = \left\{ (S, V, I) \in \mathbb{R}_{\geq 0}^3 : N \leq \max \left\{ \frac{\Lambda}{\mu}, N(0) \right\} \right\}$ .*

Since the total population remains constant, this model can be simplified by representing the susceptible population as  $S =$

$N - V - I$ , where  $N$  is the total population. Model (1) could be reduced to

$$\begin{aligned} \frac{dV}{dt} &= u_1(N - V - I) - \alpha V - \frac{\xi\beta VI}{1 + \alpha_1 I} - \mu V, \\ \frac{dI}{dt} &= \frac{\beta(N - V - I)I}{1 + \alpha_1 I} + \frac{\xi\beta VI}{1 + \alpha_1 I} - \frac{\delta I}{1 + \alpha_2 I} - \mu I. \end{aligned}$$

Then, we let  $v = V/N$ ,  $i = I/N$ ,  $b = \beta N$ ,  $a_1 = \alpha_1 N$ , and  $a_2 = \alpha_2 N$ . The result is the nondimensionalized model (1) depicted below.

$$\begin{aligned} \frac{dv}{dt} &= u_1(1 - v - i) - \alpha v - \frac{\xi b v i}{1 + a_1 i} - \mu v, \\ \frac{di}{dt} &= \frac{b(1 - v - i)i}{1 + a_1 i} + \frac{\xi b v i}{1 + a_1 i} - \frac{\delta i}{1 + a_2 i} - \mu i, \end{aligned} \tag{2}$$

with  $s = 1 - v - i$ . We could interpret  $v$  and  $i$  as the proportion of vaccinated and infected individuals, respectively, to the total population.

### 3. Model Analysis

#### 3.1. Equilibrium points

Equilibrium points are determined by setting the left-hand side of model (2) to zero. The results are as follows.

##### 1. Disease-Free Equilibrium

The DFE represents a state in which no individuals are infected, i.e., the proportion of infected individuals is zero. We have

$$DFE = (v^0, i^0) = \left( \frac{u_1}{u_1 + \alpha + \mu}, 0 \right). \tag{3}$$

##### 2. Basic Reproduction Number

The basic reproduction number, denoted as  $\mathcal{R}_0$ , is defined as the average number of new cases generated by one infected individual in a fully susceptible population [41]. This value can be calculated using the *Next-Generation Matrix* method [36]. To apply this method, we first compute the Jacobian matrix of the infected subsystem. Thus, we arrive at

$$J_1 = \left[ \begin{array}{cc} -b i + b(1 - v - i) - \mu + b v \xi + \frac{a_2 \delta i}{(1 + a_2 i)^2} - \frac{\delta}{1 + a_2 i} & \\ & \end{array} \right].$$

Following this, we decompose the Jacobian matrix  $J_1$  into its transmission and transition components, denoted as  $T$  and  $\Sigma$ . Next, we evaluate  $T$  at the DFE to obtain  $T_{DFE}$  and  $\Sigma^{-1}$ , which is the inverse of  $\Sigma$ . We have

$$\begin{aligned} T_{DFE} &= \left[ \frac{b \xi u_1}{\alpha + \mu + u_1} + b \left( 1 - \frac{u_1}{\alpha + \mu + u_1} \right) \right], \\ \Sigma^{-1} &= -\frac{1}{\delta + \mu}. \end{aligned}$$

To compute the *Next-Generation Matrix*, we use the formula  $K = -T_{DFE}\Sigma^{-1}$ , yielding  $K = \left[ \frac{b(\alpha + \mu + \xi u_1)}{(\delta + \mu)(\alpha + \mu + u_1)} \right]$ . The basic reproduction number is defined as the spectral radius of  $K$ , which is given by

$$\mathcal{R}_0 = \frac{b(\alpha + \mu + \xi u_1)}{(\delta + \mu)(\alpha + \mu + u_1)}. \tag{4}$$

##### 3. Endemic Equilibrium

The other equilibrium observed in model (2) is the endemic equilibrium, where both vaccinated and infected individuals coexist within the population. The endemic equilibrium is formally presented in **Theorem 3**.

**Theorem 3.** *The endemic equilibrium of model (2) is given by  $EE = (v^*, i^*)$  with*

$$v^* = \frac{(1 - i^*)(1 + a_1 i^*)u_1}{\alpha + \mu + b \xi i^* + u_1 + a_1 i^*(\alpha + \mu + u_1)},$$

and  $i^*$  is the solution of

$$f_1(i) = r_3 i^3 + r_2 i^2 + r_1 i + r_0 = 0,$$

where

$$\begin{aligned} r_3 &= a_2(b^2 \xi + \mu a_1^2(\alpha + \mu + u_1) + b a_1(\alpha + \mu + \xi(\mu + u_1))), \\ r_2 &= (\delta + \mu)a_1^2(\alpha + \mu + u_1) + b(b \xi + a_2(\alpha + \mu + \xi(\mu + u_1 - b))) + a_1(b(\alpha + \mu + \xi(\delta + \mu + u_1)) - a_2((b - 2\mu)(\alpha + \mu) + (b \xi - 2\mu)u_1)), \\ r_1 &= b(\alpha + \mu + \xi(\delta + \mu + u_1 - b)) + a_2((\mu - b \xi)u_1 - ((b - \mu)(\alpha + \mu))) + a_1((2\delta + 2\mu - b \xi)u_1 - ((\alpha + \mu)(b - 2(\delta + \mu)))), \\ r_0 &= u_1(\delta + \mu - b \xi) - ((b - \delta - \mu)(\alpha + \mu)). \end{aligned}$$

Typically, the endemic equilibrium occurs when  $\mathcal{R}_0 > 1$ . However, due to the endemic equilibrium's lack of explicit form, it is plausible that certain conditions, such as some value of  $\mathcal{R}_0$ , may allow for its existence even when  $\mathcal{R}_0 < 1$ . This implies that the disease could persist within the population despite expectations of its eradication.

We discuss the existence of the endemic equilibria (EE) of model (2) when both saturation effects are taken into account. Since  $r_3 > 0$ , then

$$\begin{aligned} \lim_{i \rightarrow \infty} f_1(i) &= \infty, \\ \lim_{i \rightarrow -\infty} f_1(i) &= -\infty. \end{aligned}$$

According to the Location of Roots Theorem, there is at least one  $i^*$  such that  $f_1(i^*) = 0$ . Note that when  $r_0 < 0$  or  $\mathcal{R}_0 > 1$ , there is at least one positive root of  $f_1(i)$ . This result is detailed in the next corollary.

**Corollary 1.** *If  $r_0 < 0$ , which infers  $\mathcal{R}_0 > 1$ , then there is at least one endemic equilibrium of model (2).*

The remaining analysis is conducted using a gradient analysis. The Descartes' Rule of Sign of  $f_1(i)$  is summarized in **Table 1**.

By applying gradient analysis, we implicitly differentiate  $f_1(i)$  with respect to  $\mathcal{R}_0$  and evaluate it at  $i = 0$  and  $\mathcal{R}_0 = 1$ . This results in  $r_1 \frac{\partial i}{\partial \mathcal{R}_0} + \frac{\partial r_0}{\partial \mathcal{R}_0}$ . The condition  $\frac{\partial i}{\partial \mathcal{R}_0} < 0$  holds

**Table 1.** Descartes' Rule of Sign of  $f_1(i)$

Case	$r_3$	$r_2$	$r_1$	$r_0$	$\mathcal{R}_0$	Possible Positive Roots
1	+	+	+	+	$\mathcal{R}_0 < 1$	0
2	+	+	+	-	$\mathcal{R}_0 > 1$	1
3	+	+	-	+	$\mathcal{R}_0 < 1$	0 or 2
4	+	+	-	-	$\mathcal{R}_0 > 1$	1
5	+	-	+	+	$\mathcal{R}_0 < 1$	0 or 2
6	+	-	+	-	$\mathcal{R}_0 > 1$	1 or 3
7	+	-	-	+	$\mathcal{R}_0 < 1$	0 or 2
8	+	-	-	-	$\mathcal{R}_0 > 1$	1

if  $-\frac{1}{r_1} \frac{\partial r_0}{\partial \mathcal{R}_0} < 0$ . Thus, EE exist when  $\mathcal{R}_0 < 1$  and

$$a_2 > \frac{1}{\delta(\alpha + \mu + \xi u_1)^2} \left[ (\delta + \mu)(a_1(\alpha + \mu + \xi u_1)^2 + (\alpha + \mu + \xi(\delta + \mu + u_1))(\alpha + \mu + \xi u_1) - (\delta + \mu)\xi(\alpha + \mu + u_1)) \right].$$

This result is formalized in the following theorem.

**Theorem 4.** The EE of model (2) exists for some value of  $\mathcal{R}_0 < 1$ , if

$$a_2 > \frac{1}{\delta(\alpha + \mu + \xi u_1)^2} \left[ (\delta + \mu)(a_1(\alpha + \mu + \xi u_1)^2 + (\alpha + \mu + \xi(\delta + \mu + u_1))(\alpha + \mu + \xi u_1) - (\delta + \mu)\xi(\alpha + \mu + u_1)) \right].$$

Since the polynomial for the existence of the endemic equilibrium of the complete model is due to the third-degree polynomial, it is difficult to determine the range of  $\mathcal{R}_0$  such that the model has more than one endemic equilibrium for some value of  $\mathcal{R}_0 < 1$ . This allows us to analyze a simple case where only transmission saturation is considered, or  $a_2 = 0$ . Model (2) when  $a_2 = 0$  is rewritten as:

$$\begin{aligned} \frac{dv}{dt} &= u_1(1 - v - i) - \alpha v - \frac{\xi bvi}{1 + a_1 i} - \mu v, \\ \frac{di}{dt} &= \frac{b(1 - v - i)i}{1 + a_1 i} + \frac{\xi bvi}{1 + a_1 i} - \delta i - \mu i. \end{aligned} \tag{5}$$

The endemic equilibrium of this model is stated in Theorem 5.

**Theorem 5.** Special case when  $a_2 = 0$ . The endemic equilibrium of model (5) is given by  $EE_2 = (v_2^*, i_2^*)$  with

$$v = \frac{b(1 - i_2^*) - (\delta + \mu + i_2^*(\delta + \mu)a_1)}{b(1 - \xi)},$$

and  $i_2^*$  is the solution of

$$f_2(i) = q_2 i^2 + q_1 i + q_0 = 0,$$

where

$$\begin{aligned} q_2 &= b^2 \xi + (\delta + \mu)a_1^2(\alpha + \mu + u_1) + ba_1(\alpha + \mu + \xi(\delta + \mu + u_1)), \\ q_1 &= b(\alpha + \mu + \xi(\delta + \mu + u_1 - b)) + a_1(u_1(2\delta + 2\mu - b\xi) - ((\alpha + \mu)(b - 2(\delta + \mu)))), \\ q_0 &= u_1(\delta + \mu - b\xi) - ((b - \delta - \mu)(\alpha + \mu)). \end{aligned}$$

Next, we discuss the existence of the EE of model (5). Note that we have the endemic equilibrium of the second-degree polynomial, represented by  $f_2(i)$ , which indicates that there might be two EE. By employing a gradient analysis, the implicit derivative of  $f_2(i)$  is evaluated at  $i = 0$ , and  $\mathcal{R}_0 = 1$  is given by  $q_1 \frac{\partial i}{\partial \mathcal{R}_0} + \frac{\partial q_0}{\partial \mathcal{R}_0}$ . This leads to  $\frac{\partial i}{\partial \mathcal{R}_0} = -\frac{1}{q_1} \frac{\partial q_0}{\partial \mathcal{R}_0}$ . Thus, we find that two EE exist when  $\frac{\partial i}{\partial \mathcal{R}_0} < 0$  or when  $\mathcal{R}_0 < 1$  if

$$a_1 < \frac{\xi u_1(\delta(1 - \xi) - 2\alpha - \mu(1 + \xi)) - ((\alpha + \mu)^2 + \xi^2 u_1^2)}{(\alpha + \mu + \xi u_1)^2}.$$

This result is stated in the next theorem.

**Theorem 6.** Let

$$a_1^* = \frac{\xi u_1(\delta(1 - \xi) - 2\alpha - \mu(1 + \xi)) - ((\alpha + \mu)^2 + \xi^2 u_1^2)}{(\alpha + \mu + \xi u_1)^2}.$$

The EE of model (5), has:

- (a) no endemic equilibrium when  $\mathcal{R}_0 < 1$  and  $a_1 > a_1^*$ ,
- (b) one endemic equilibrium for any  $\mathcal{R}_0 > 1$ ,
- (c) twin EE at  $\mathcal{R}_0 = \mathcal{R}_0^c < 1$  and  $a_1 < a_1^*$ , where  $\mathcal{R}_0^c$  is  $\mathcal{R}_0$  that satisfies  $q_1^2 - 4q_2 q_0 = 0$ , or
- (d) two different equilibria at  $\mathcal{R}_0^c < \mathcal{R}_0 < 1$  and  $a_1 < a_1^*$ .

### 3.2. Stability Analysis

#### 1. Stability of Disease-Free Equilibrium

The Jacobian matrix evaluated at the DFE is given by:

$$\begin{aligned} J|_{DFE} &= \begin{bmatrix} J_{11} & J_{12} \\ 0 & J_{22} \end{bmatrix}, \\ J_{11} &= -(\alpha + \mu + u_1), \quad J_{12} = -\left(u_1 + \frac{b\xi u_1}{\alpha + \mu + u_1}\right), \\ J_{22} &= -\delta - \mu + \frac{b\xi u_1}{\alpha + \mu + u_1} + b\left(1 - \frac{u_1}{\alpha + \mu + u_1}\right). \end{aligned}$$

The characteristic equation of  $J_{DFE}$  is  $P(\lambda) = \lambda^2 + B\lambda + C$ , where

$$\begin{aligned} B &= -b + \alpha + \delta + 2\mu + u_1 + \frac{bu_1(1 - \xi)}{\alpha + \mu + u_1}, \\ C &= -(\delta + \mu)(\alpha + \mu + u_1)(\mathcal{R}_0 - 1). \end{aligned}$$

It follows that for  $P(\lambda)$  to have two roots with the same sign, we require  $C > 0$ , which implies  $-(\mathcal{R}_0 - 1) > 0$ . Thus, when  $\mathcal{R}_0 < 1$ , the eigenvalues are of the same sign. To ensure that  $P(\lambda)$  has two negative roots, we need  $B > 0$ ,

or

$$\begin{aligned}
 b - \frac{bu_1(1-\xi)}{\alpha + \mu + u_1} &< \alpha + \delta + 2\mu + u_1, \\
 b &< \frac{(\alpha + \delta + 2\mu + u_1)(\alpha + \mu + u_1)}{\alpha + \mu + \xi u_1}, \\
 \frac{\mathcal{R}_0(\delta + \mu)(\alpha + \mu + u_1)}{\alpha + \mu + \xi u_1} &< \frac{(\alpha + \delta + 2\mu + u_1)(\alpha + \mu + u_1)}{\alpha + \mu + \xi u_1}, \\
 \mathcal{R}_0(\delta + \mu) &< \alpha + \delta + 2\mu + u_1, \\
 \mathcal{R}_0 &< 1 + \frac{\alpha + \mu + u_1}{\delta + \mu}.
 \end{aligned}$$

Since  $\mathcal{R}_0 < 1 < 1 + \frac{\alpha + \mu + u_1}{\delta + \mu}$ , this guarantees that both eigenvalues are negative when  $\mathcal{R}_0 < 1$ .

**Theorem 7.** *The DFE is locally asymptotically stable if  $\mathcal{R}_0 < 1$  and unstable if  $\mathcal{R}_0 > 1$ .*

### 2. Stability of Endemic Equilibrium

To analyze the stability of the endemic equilibrium, we employ the Castillo-Song Theorem that is based on central manifold theory [42]. We now discuss the stability analysis of the endemic equilibrium of model (2) by rewriting model (2) with  $v = x_1$  and  $i = x_2$ . The rewritten version of model (2) is as follows:

$$\begin{aligned}
 g_1 &= \frac{dx_1}{dt} = u_1(1 - x_1 - x_2) - \alpha x_1 - \frac{\xi b x_1 x_2}{1 + a_1 x_2} - \mu x_1, \\
 g_2 &= \frac{dx_2}{dt} = \frac{b(1 - x_1 - x_2)x_2}{1 + a_1 x_2} + \frac{\xi b x_1 x_2}{1 + a_1 x_2} - \frac{\delta x_2}{1 + a_2 x_2} - \mu x_2.
 \end{aligned} \tag{6}$$

The Jacobian matrix of this system is given as:

$$\begin{aligned}
 J_3 &= \begin{bmatrix} J3_{11} & J3_{12} \\ J3_{21} & J3_{22} \end{bmatrix}, \\
 J3_{11} &= -\left(\alpha + \mu + \frac{bx_2\xi}{1 + a_1x_2} + u_1\right), \\
 J3_{12} &= -\left(\frac{bx_1\xi}{(1 + a_1x_2)^2} + u - 1\right), \\
 J3_{21} &= -\frac{bx_2(1 - \xi)}{1 + a_1x_2}, \\
 J3_{22} &= -\mu - \frac{\delta}{(1 + a_2x_2)^2} + \frac{b(1 - (1 - \xi)x_1 - x_2)}{(1 + a_1x_2)^2}.
 \end{aligned}$$

This Jacobian matrix evaluated at DFE and

$$b = b^* = \frac{(\delta + \mu)(\alpha + \mu + u_1)}{\alpha + \mu + \xi u_1}$$

is given by:

$$J_3|_{DFE, b=b^*} = \begin{bmatrix} -\alpha - \mu - u_1 & -u_1 \left(1 + \frac{(\delta + \mu)\xi}{\alpha + \mu + \xi u_1}\right) \\ 0 & 0 \end{bmatrix}.$$

The eigenvalues of this matrix are  $\lambda_1 = 0$  and  $\lambda_2 = -\alpha - \mu - u_1$ . The presence of a zero eigenvalue and a negative

eigenvalue satisfies the first assumption of the Castillo-Song Theorem. Next, we determine the right and left eigenvectors of  $J_3|_{DFE, b=b^*}$ . The right eigenvector is defined as  $v = (v_1, v_2)^T$ . By solving  $J_3|_{DFE, b=b^*}v = 0$ , we obtain

$$v_1 = \frac{-v_2 u_1 (\alpha + \mu + \xi (\delta + \mu + u_1))}{(\alpha + \mu + u_1)(\alpha + \mu + \xi u_1)}.$$

To simplify the calculation, we let

$$\begin{aligned}
 v_1 &= -u_1(\alpha + \mu + \xi(\delta + \mu + u_1)), \\
 v_2 &= (\alpha + \mu + u_1)(\alpha + \mu + \xi u_1).
 \end{aligned}$$

The left eigenvector is represented as  $w = (w_1, w_2)$ , where  $w_1 = 0$  and  $w_2 > 0$  after solving  $wJ_3|_{DFE, b=b^*} = 0$ . The existence of a right eigenvector with nonnegative component corresponding to the zero entries of DFE, along with a left eigenvector, fulfills the second assumption of the Castillo-Song Theorem. By using the formula in the theorem to obtain  $a$  and  $b$ , we arrive at the non-zero partial derivatives:

$$\begin{aligned}
 \frac{\partial^2 g_2}{\partial x_1 \partial x_2} &= \frac{\partial^2 g_2}{\partial x_2 \partial x_1} \\
 &= -\frac{(\delta + \mu)(1 - \xi)(\alpha + \mu + u_1)}{\alpha + \mu + \xi u_1}, \\
 \frac{\partial^2 g_2}{\partial x_2^2} &= -2(\delta + \mu)a_1 + 2\delta a_2 - \frac{2(\delta + \mu)(\alpha + \mu + u_1)}{\alpha + \mu + \xi u_1}, \\
 \frac{\partial^2 g_2}{\partial x_2 \partial b} &= \frac{\alpha + \mu + \xi u_1}{\alpha + \mu + u_1},
 \end{aligned}$$

we obtain

$$\begin{aligned}
 a &= w_2(\alpha + \mu + u_1)^2 \times \left(2(\delta + \mu)(1 - \xi)u_1(\alpha + \mu + \xi(\delta + \mu + u_1)) - (\alpha + \mu + \xi u_1)^2 \left(2(\delta + \mu)a_1 - 2\delta a_2 + \frac{2(\delta + \mu)(\alpha + \mu + u_1)}{\alpha + \mu + \xi u_1}\right)\right), \\
 b &= w_2(\alpha + \mu + \xi u_1)^2 > 0.
 \end{aligned} \tag{7}$$

The condition  $a > 0$  infers the occurrence of a backward bifurcation. Thus, we conclude that:

**Theorem 8.** *Model (2) experiences backward bifurcation at  $\mathcal{R}_0 = 1$ , if  $a > 0$ .*

### 3. Global Stability Analysis

Another question worth addressing is whether the system possesses closed orbits within the solution region. If it possesses closed orbits, then there would be periodic solutions at certain parameter values. To examine this, we employ Dulac's Criterion [43]. Let

$$R = \{(x_1, x_2) : x_1 \in [0, 1], x_2 \in (0, 1]\}.$$

We consider the function  $h = \frac{1}{x_2}$ . Then, we obtain

$$hg_1 = \frac{1}{x_2} \left(-(\alpha + \mu)x_1 + u_1(1 - x_1 - x_2) - \frac{bx_1x_2}{1 + a_1x_2}\right),$$

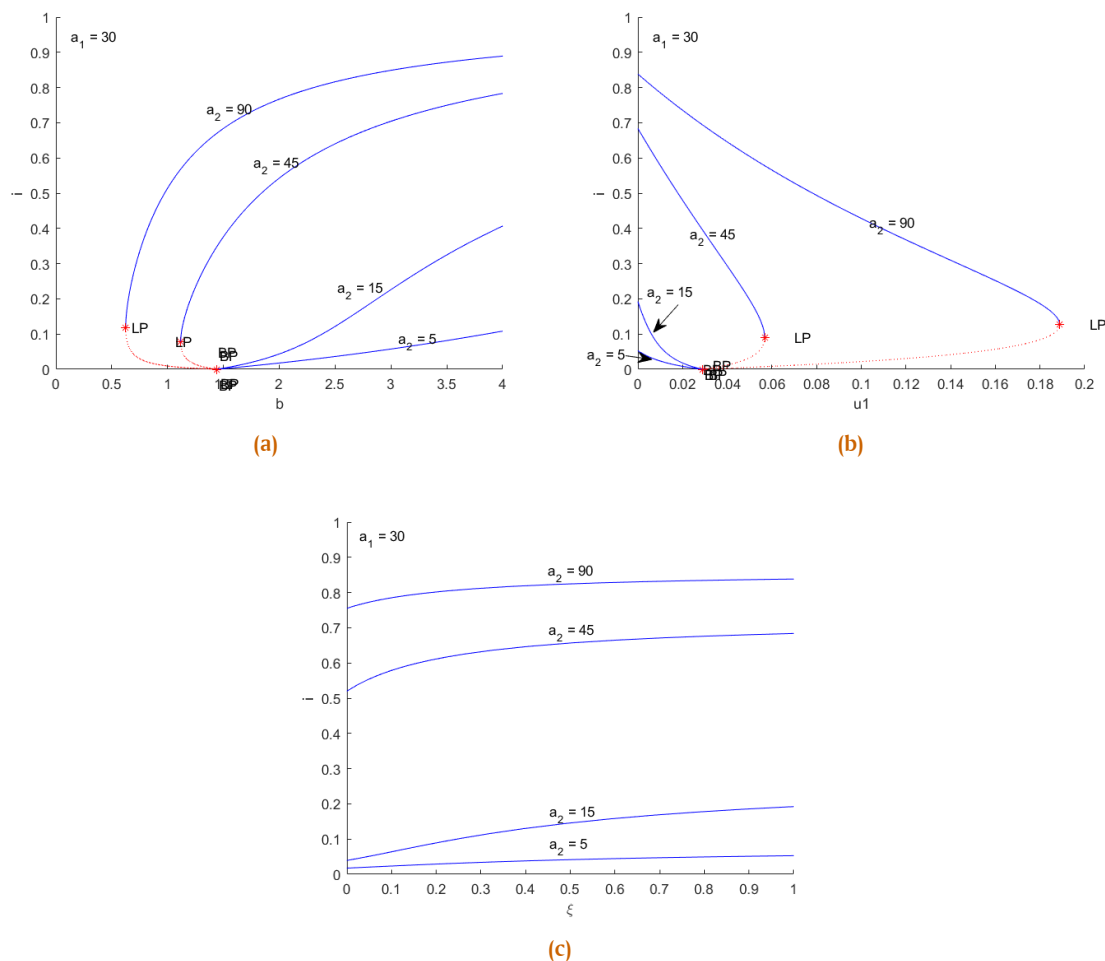


**Figure 2.** Bifurcation diagram of model in (2) using of  $b$ ,  $u_1$ , and  $\xi$  as the bifurcation parameter shown in panel (a), (b), and (c), respectively.  $LP$  and  $BP$  denotes the fold and branching point, respectively. All parameters remain constant, except  $a_2$  which varies.

$$hg_2 = \frac{1}{x_2} \left( -\mu x_2 + \frac{b\xi x_1 x_2}{1 + a_1 x_2} + \frac{b(1 - x_1 - x_2)x_2}{1 + a_1 x_2} - \frac{\delta x_2}{1 + a_2 x_2} \right).$$

We have

$$\begin{aligned} \frac{\partial(hg_1)}{\partial x_1} + \frac{\partial(hg_2)}{\partial x_2} &= \frac{\delta a_2}{(1 + a_2 x_2)^2} - \frac{\alpha + \mu + u_1}{x_2} \\ &\quad - \frac{b(1 + a_1 + \xi + a_1 x_1(1 - \xi) + \xi a_1 x_2)}{(1 + a_1 x_2)^2}, \\ &= \frac{1}{x_2(1 + a_1 x_2)^2(1 + a_2 x_2)^2} \left[ -(\alpha + \mu + u_1)(1 + a_1 x_2)^2(1 + a_2 x_2)^2 - b(1 + a_1 + \xi + a_1 x_1(1 - \xi) + \xi a_1 x_2)x_2(1 + a_2 x_2)^2 + \delta a_2 x_2(1 + a_1 x_2)^2 \right]. \end{aligned}$$

To ensure that  $\frac{\partial(hg_1)}{\partial x_1} + \frac{\partial(hg_2)}{\partial x_2}$  have the same sign, specifically  $\frac{\partial(hg_1)}{\partial x_1} + \frac{\partial(hg_2)}{\partial x_2} < 0$ , we require:

$$\begin{aligned} \delta a_2 x_2(1 + a_1 x_2)^2 &< (\alpha + \mu + u_1)(1 + a_1 x_2)^2(1 + a_2 x_2)^2 \\ &\quad + b(1 + a_1 + \xi + a_1 x_1(1 - \xi) \\ &\quad + \xi a_1 x_2)x_2(1 + a_2 x_2)^2. \end{aligned}$$

This inequality can be further rearranged and simplified as:

$$\frac{\mathcal{R}_0(\delta + \mu)x_2(1 + a_2 x_2)^2}{\alpha + \mu + \xi u_1} [1 + a_1 + \xi + a_1 x_1(1 - \xi) + \xi a_1 x_2] > \frac{1}{(\alpha + \mu + u_1)(1 + a_2 x_2)^2} \left[ (1 + a_1 x_2)^2(\delta a_2 x_2 - (\alpha + \mu + u_1)(1 + a_2 x_2)^2) \right].$$

Given that  $(x_1, x_2) \in R$ , we get

$$\frac{\mathcal{R}_0(\delta + \mu)(1 + 2a_1 + \xi)}{\alpha + \mu + \xi u_1} > \frac{\mathcal{R}_0(\delta + \mu)x_2(1 + a_2 x_2)^2}{\alpha + \mu + \xi u_1} [1 + a_1 + \xi + a_1 x_1(1 - \xi) + \xi a_1 x_2]$$

and

$$\frac{(1 + a_1 x_2)^2 (\delta a_2 x_2 - (\alpha + \mu + u_1)(1 + a_2 x_2)^2)}{(\alpha + \mu + u_1)(1 + a_2 x_2)^2} > -\frac{1}{(1 + a_2)^2}.$$

Thus, it follows that

$$\mathcal{R}_0 > -\frac{(\alpha + \mu + \xi u_1)}{(\delta + \mu)(1 + 2a_1 + \xi)(1 + a_2)^2}.$$

Therefore, when  $\mathcal{R}_0 > 0$ , by Dulac's Criterion, there are no closed orbits in  $R$ . The result is stated in the next theorem.

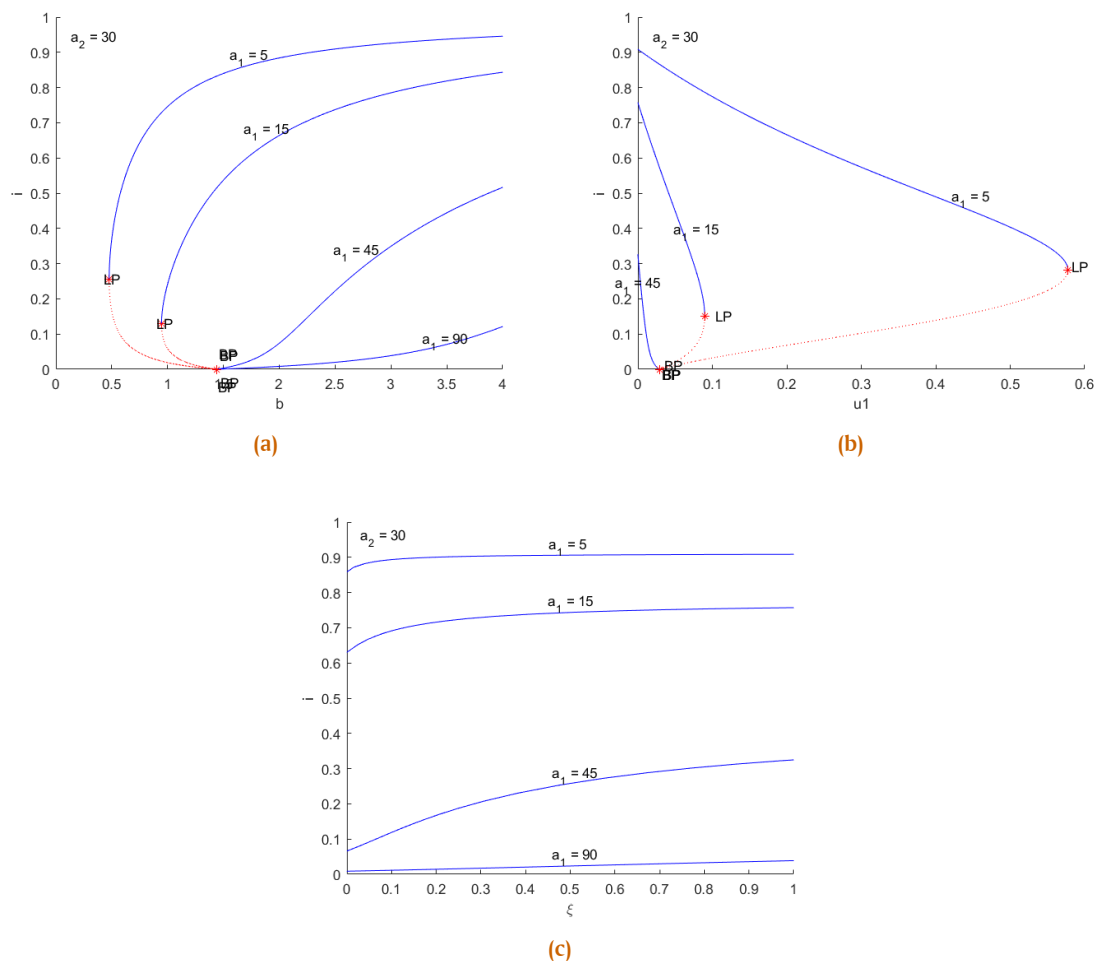


**Figure 3.** Bifurcation diagram of model in (2) using of  $b$ ,  $u_1$ , and  $\xi$  as the bifurcation parameter shown in panel (a), (b), and (c), respectively. All parameters remain constant, except  $a_1$  which varies.

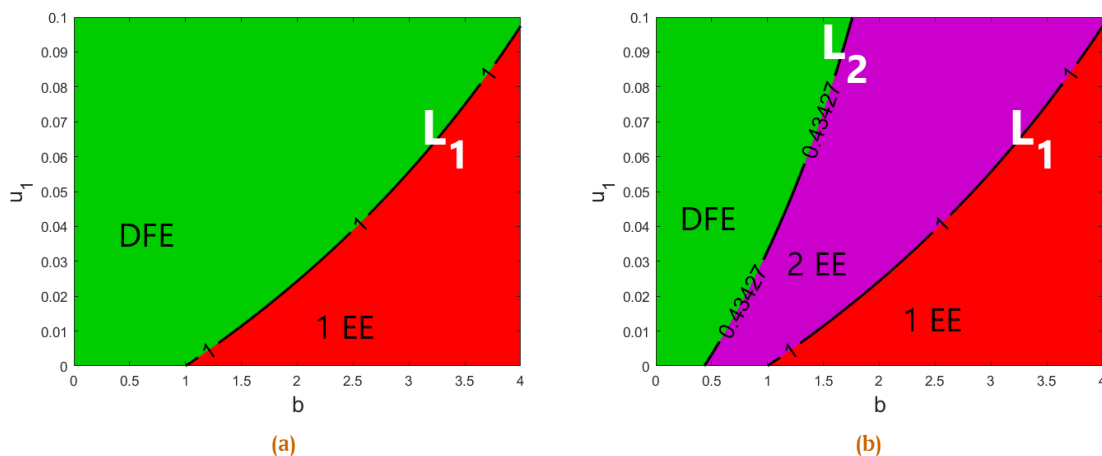


**Figure 4.** Bifurcation diagrams in the  $b$ - $u_1$  plane illustrate the scenarios in which forward bifurcation (panel (a)) or backward bifurcation (panel (b)) occurs. In these diagrams, the green region represents the parameter space where the DFE is the only stable equilibrium. The purple region corresponds to the coexistence of two EE (one stable and one unstable) alongside a stable DFE, indicating bistability. The red region denotes the parameter space where only one endemic equilibrium exists, which is stable. The  $L_1$  line represents the condition  $\mathcal{R}_0 = 1$ , while  $L_2$  corresponds to  $\mathcal{R}_0 = 0.43427$ , which is the fold point where backward bifurcation arises.

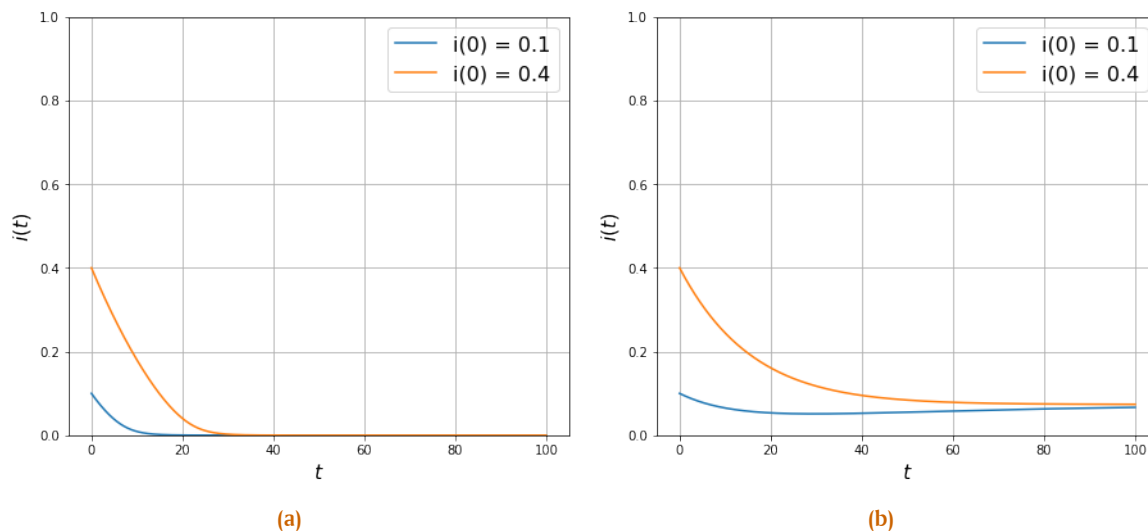


Figure 5. Autonomous simulation of forward bifurcation

**Theorem 9.** Model (2) possesses no closed orbits in  $R$ .

Consequently, the endemic equilibrium of model (2) is globally stable. This is only valid if the endemic equilibrium exists in the solution region.

### 3.3. Discussion from the analytical results

We proposed our SVI model in eq. (1) which later can be simplified into a two dimensional-*vi* model by assuming the total population is constant. The analytical results are widely covered the dynamical properties of the model, ranging from the positivity criteria, existence of equilibrium points, up to the stability of the equilibrium points. We have shown from Theorem 3 and 4 that the basic reproduction number determines the existence of the endemic equilibrium. Caused by saturated infection and treatment, our model shows a possibility to have more than one endemic equilibrium, especially when the basic reproduction number is less than one. This phenomena later confirmed by Theorem 8 that our model may exhibit a backward bifurcation at basic reproduction number equal to one if the saturation parameter in infection or treatment term exceed some threshold, particularly when  $a_1 < a_1^*$  and  $a_2 > a_2^*$ .  $a_1 < a_1^*$  indicates that the model exhibit backward bifurcation if the saturation parameter in transmission term is less than the threshold, inferring that if the transmsion is not significantly reduced given the increasing infected population, then the endemic equilibrium still persist in the population even when  $\mathcal{R}_0 < 1$ . Similarly,  $a_2 > a_2^*$  indicates that the model exhibit backward bifurcation if the saturation parameter in treatment term is greater than the threshold, inferring that if the recovery rate is significantly reduce given the increasing infected population (which also infers the prolonged recovery time), the endemic equilibrium still persist in the population even when  $\mathcal{R}_0 < 1$ . These findings imply that achieving disease control requires more than simply reducing the basic reproduction number below one, as the presence of backward bifurcation and saturation effects can sustain endemic levels. This highlights the need for targeted interventions that address these nonlinear

dynamics to ensure successful disease eradication.

## 4. Numerical Simulation

### 4.1. Bifurcation Diagram and Autonomous Simulation

This section is dedicated to plotting the bifurcation diagram of model (2) for selected parameters, namely the infection parameter  $b$ , rate of vaccination  $u_1$ , and vaccine efficacy  $\xi$ , under varying values of the saturation effects  $a_1$  and  $a_2$ . By utilizing the parameter values outlined in Table 2, we can calculate the critical values of  $a_1$  and  $a_2$  that may determine the type of bifurcation, i.e.,  $a_1^* = 31.1346$  and  $a_2^* = 28.8651$ . Hence, according to Theorem 8, if  $a_2 > a_2^*$ , a backward bifurcation may occur. Conversely, if  $a_2 < a_2^*$ , the model will always undergo a forward bifurcation at  $\mathcal{R}_0 = 1$ . Similarly, if  $a_1 < a_1^*$ , a backward bifurcation appears at  $\mathcal{R}_0 = 1$ . The diagrams are depicted in Figures 2 and 3.

Table 2. Parameter values used in numerical simulation in Figures 2 and 3.

Parameter	Description	Value	Source
$u_1$	Vaccination rate	0.01	[11]
$\alpha$	Loss of vaccine effectiveness	$\frac{1}{52}$	Assumed
$\xi$	Reduction due to vaccine efficacy	0.01	Assumed
$\mu$	Natural death rate	$\frac{1}{72 \times 52}$	[44]
$\delta$	Recovery rate	1	[11]
$b$	Transmission rate	2.159182	Assumed

The effect of varying  $a_2$  using  $b$ ,  $u_1$ , or  $\xi$  as the bifurcation parameter is illustrated in Figure 2. In Figure 2a, the bifurcation diagram using  $b$  as the bifurcation parameter under variation of  $a_1$  where  $a_1 = 5$  and  $a_2 = 15$  shows a forward bifurcation at  $\mathcal{R}_0 = 1$ , while  $a_2 = 45$  and  $a_2 = 90$  result in a backward bifurcation at  $\mathcal{R}_0 = 1$ . A similar analysis can be applied to Figure 2b when  $u_1$  is the bifurcation parameter. On the other hand, Figure 2c demonstrates the scenario when  $\xi$  as the bifurcation parameter, revealing that no  $\xi \in [0, 1]$  can yield  $\mathcal{R}_0 = 1$ . Hence, the bifurcation diagram in Figure 2c for  $\xi \in [0, 1]$  does not exhibit the Branching Point (BP). However, our findings using  $\xi$  as the bifurcation parameter remains consistent with Figures 2a and 2b, indicating that a larger value of  $a_2$  results in a higher size of en-

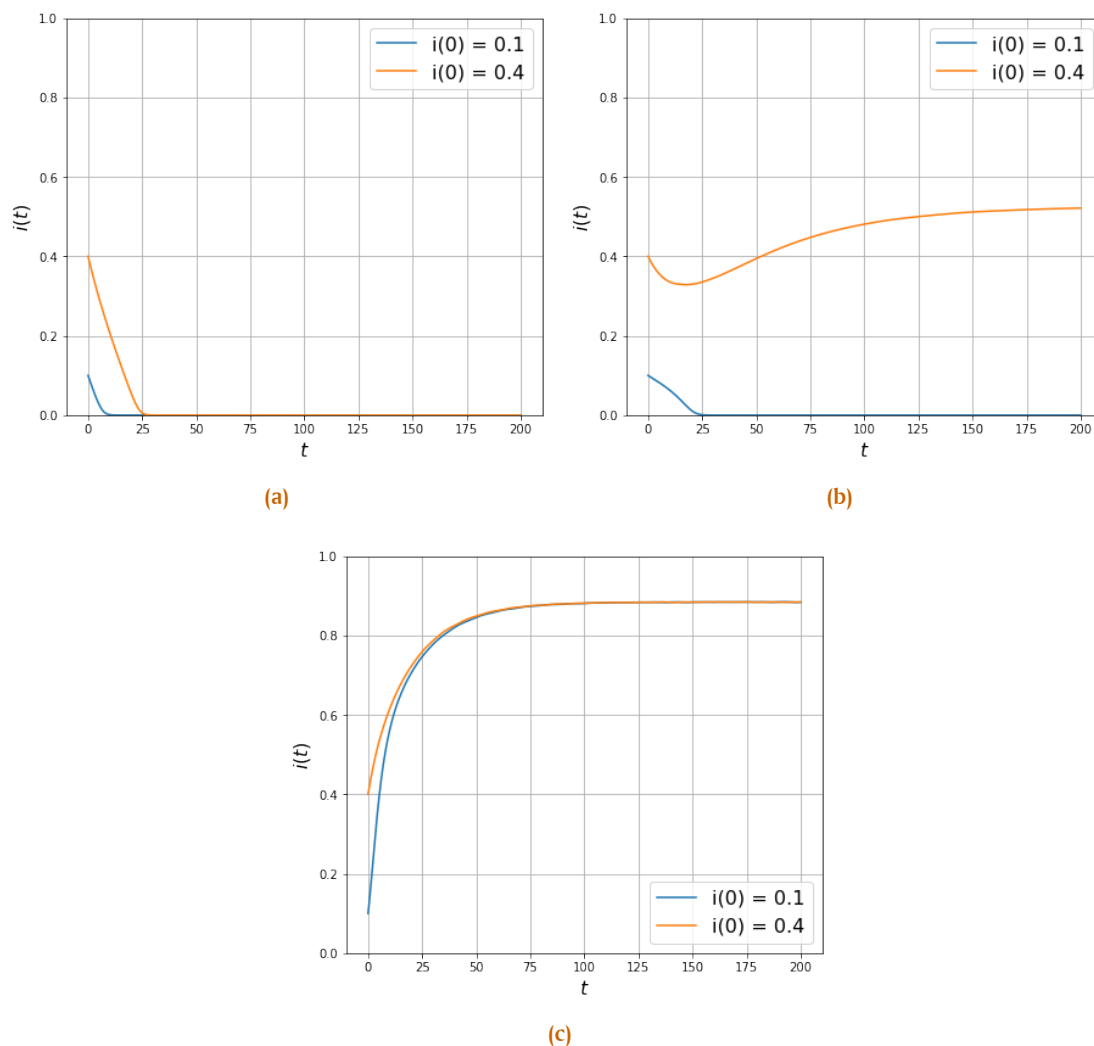


**Figure 6.** Autonomous simulations in the presence of backward bifurcation phenomenon demonstrate that the solution depends on the initial conditions. The results show that the solutions converge to the same stable disease-free equilibrium in panel (a), to different equilibria (disease-free and endemic equilibrium) in panel (b), and to the same endemic equilibrium in panel (c).

demographic equilibrium. For  $b < b^* = 1.439454522$ , where  $b^*$  is the BP satisfying  $\mathcal{R}_0 = 1$ , and  $a_2 = 5$  or  $a_2 = 15$ , when forward bifurcation at  $\mathcal{R}_0 = 1$  occurs, the system exhibits a stable DFE. When  $b$  reaches the BP at  $b^*$ , the DFE transitions from stable to unstable. Simultaneously, a stable endemic equilibrium emerges and continues to grow as  $b$  increases. Consequently, for  $b > b^*$ , the model displays a stable endemic equilibrium and an unstable DFE.

A different phenomenon unfolds when  $a_2 = 45$ , resulting in a backward bifurcation at  $\mathcal{R}_0 = 1$ , as shown in Figure 2a. Beginning with the branch denoted by stable endemic equilibrium when  $b > b^*$ . When  $b > b^*$ , a unique stable endemic equilibrium, represented by the blue curves, coexists with an unstable DFE. As  $b$  decreases, the size of the endemic equilibrium continues to diminish until it reaches the fold point at  $b^+ = 0.56726882$ . Beyond this point ( $b^+$ ), the stability of the endemic equilibrium branch shifts from stable to unstable. As  $b$  increases along this unstable branch, the endemic equilibrium size of  $i$  decreases until it meets the BP at  $b = b^*$ . At this BP, the stability of the DFE changes: if  $b$  is smaller than the BP, the DFE is stable; if  $b$  is larger

than the BP, the DFE becomes unstable. A similar argument applies to the case where  $a_2 = 45$ , or other scenarios illustrated in Figure 2b.

The next set of simulations is presented in Figure 3, utilizing the same bifurcation parameter while varying  $a_1$  to determine the type of bifurcation at  $\mathcal{R}_0 = 1$ , whether it is a forward or backward bifurcation. The BP  $b_1 = 1.439454522$  is identified at  $\mathcal{R}_0 = 1$ . Unlike the previous simulations in Figure 2, where increasing  $a_2$  increases the likelihood of a backward bifurcation, the simulations in Figure 3 demonstrate that increasing  $a_1$  decreases the probability of a backward bifurcation at  $\mathcal{R}_0 = 1$ . It is evident that selecting  $a_1 = 45$  or  $a_1 = 90$  results in a forward bifurcation at  $\mathcal{R}_0 = 1$ , while choosing  $a_1 = 5$  or  $a_1 = 15$  leads to a backward bifurcation at  $\mathcal{R}_0 = 1$ . Hence, a smaller saturation effect increases the likelihood of having a stable endemic equilibrium point, even when the basic reproduction number is less than one.

The next simulation is presented in Figure 4, illustrating the two-parameter regions for the existence and stability of equilibrium points. We use  $b$  and  $u_1$  as bifurcation parameters, setting

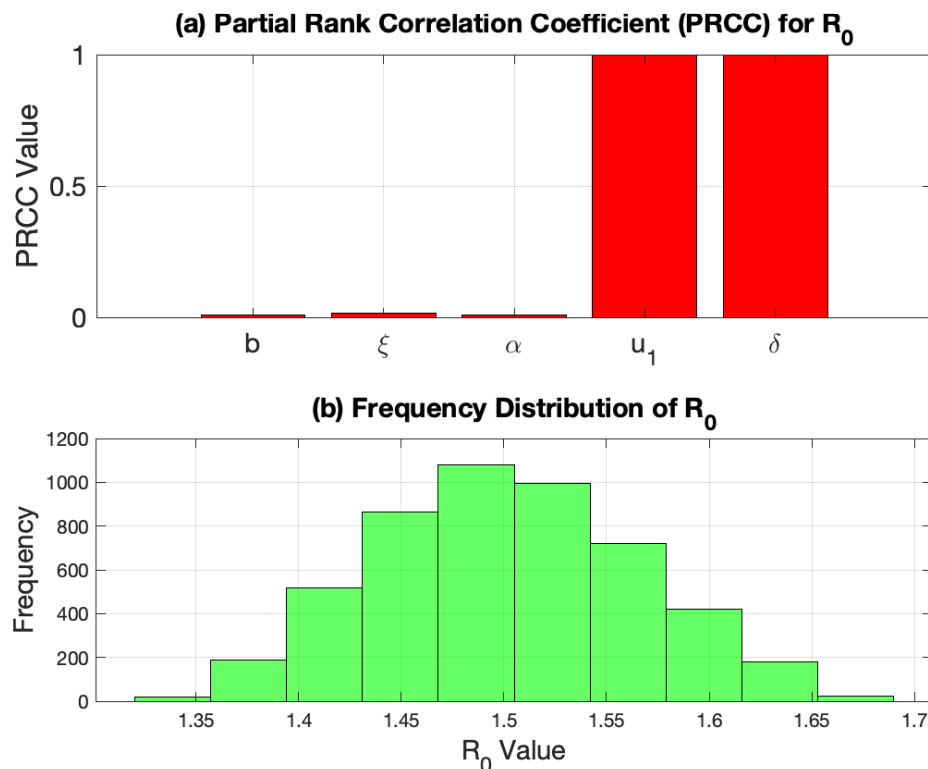


Figure 7. Global sensitivity analysis of parameter values in Table 2.

$a_1 = 45$  and  $a_2 = 30$  to produce Figure 4a, and  $a_1 = 5$  and  $a_2 = 30$  to produce Figure 4b. In Figure 4a, which depicts forward bifurcation phenomenon, the  $b-u_1$  plane is divided into two regions by the line  $L_1$ , corresponding to  $R_0 = 1$ . The green area, where  $R_0 < 1$ , represents the parameter space where only a stable DFE exists, and no endemic equilibrium is present. Conversely, the red area, where  $R_0 > 1$ , corresponds to the existence of a unique stable endemic equilibrium, while the DFE becomes unstable. In contrast, Figure 4b depicts a scenario where the phenomenon of backward bifurcation occurs, dividing the plane into three regions. The red region, where  $R_0 > 1$ , represents the parameter space where the DFE is unstable, and a unique endemic equilibrium is stable. The purple region, lying between lines  $L_1$  and  $L_2$ , indicates the presence of two stable equilibria (a stable DFE and a stable endemic equilibrium) and one unstable endemic equilibrium, signifying bistability. Finally, the green region, where  $R_0 < L_2$  (with  $L_2$  denoting the fold point where backward bifurcation occurs), represents the parameter space where only a stable DFE exists.

Next, we perform autonomous simulations to demonstrate the dynamics of our model over time. For this purpose, we substitute the parameter values from Table 2 into our model in (2). The only parameter that varies during the simulation is  $b$ . To illustrate both forward and backward bifurcation, we set  $a_2 = 30$ , with  $a_1 = 45$  for forward bifurcation and  $a_1 = 5$  for backward bifurcation. The simulations are conducted using two initial conditions:  $(v(0), i(0)) = (0.4, 0.1)$  and  $(v(0), i(0)) = (0.4, 0.4)$ . The numerical results are shown in Figure 5 when forward bifurcation appears and Figure 6 when backward bifurcation appears.

In Figure 5a, when  $b$  is chosen such that  $R_0 < 1$  (e.g.,

$b = 0.5$ ), the solution of model (2), particularly  $i(t)$ , converges to zero, representing the DFE, regardless of the initial condition. Conversely, when  $b$  is chosen such that  $R_0 > 1$  (e.g.,  $b = 1.5$ ), the solution converges to the endemic equilibrium, regardless of the initial condition, as shown in Figure 5b. These results confirm the model analysis: when the model undergoes forward bifurcation, the solution will approach the DFE when  $R_0 < 1$  and the endemic equilibrium when  $R_0 > 1$ .

In Figure 6, a consistent pattern emerges when  $b$  is chosen such that  $R_0 > 1$  (e.g.,  $b = 1.5$ ) or  $R_0 < R_0^c$  (e.g.,  $b = 0.25$ ). In the former scenario, the solution converges to the endemic equilibrium, as shown in Figure 6c, while in the latter case, it converges to the DFE, as shown in Figure 6a. Since the model exhibits backward bifurcation, where selecting  $b$  such that  $R_0^c < R_0 < 1$  (e.g.,  $b = 0.75$ ) results in the solution being dependent on the initial condition. If the initial condition is closer to the DFE (e.g.,  $i(0) = 0.1$ ), the solution will converge to the DFE. Conversely, if the initial condition is closer to the endemic equilibrium (e.g.,  $i(0) = 0.4$ ), the solution will converge to the endemic equilibrium. This indicates the occurrence of bistability in backward bifurcation when  $R_0^c < R_0 < 1$ , as illustrated in Figure 6b.

#### 4.2. Sensitivity Analysis

We conduct a global sensitivity analysis in this section using Partial Rank Correlation Coefficient (PRCC) with the Latin Hypercube Sampling (LHS) method. We take 5000 sample points from the parameter values in Table 2, ranging between 95% and 105% of the parameter values listed in Table 2. The results are presented in Figure 7. It is clear that with this set of parameter values, the

vaccination intervention ( $u_1$ ) and recovery rate ( $\delta$ ) are the most sensitive parameters impacting  $\mathcal{R}_0$ , followed by vaccine efficacy  $\xi$ , infection rate  $b$ , and vaccine drop out  $\alpha$ , respectively. Furthermore, from the 5000 sample point that we use, the  $\mathcal{R}_0$  ranges between 1.35 to 1.7, with  $\mathcal{R}_0 = 1.5$  being the most frequent  $\mathcal{R}_0$ .

## 5. Conclusion

This article discusses a source of backward bifurcation related to saturation effects in infection and treatment rates within an imperfect vaccination model. The model was constructed using a Susceptible-Vaccinated-Infected-Susceptible (SVIS) compartmental framework and simplified to a system of two nonlinear differential equations by assuming a constant population size. The paper demonstrates the existence of a unique solution and analyzes the existence and stability of the DFE and EE analytically. The basic reproduction number,  $\mathcal{R}_0$ , was calculated to assess whether the epidemic would converge to the disease-free or endemic equilibrium.

The analysis reveals that at least one endemic equilibrium exists when  $\mathcal{R}_0 > 1$ , and under certain conditions, an endemic equilibrium may also exist even when  $\mathcal{R}_0 < 1$ , indicating the occurrence of a backward bifurcation. This phenomenon is attributed to saturation effects in the infection and recovery terms. A smaller value of the saturation parameter for infection term increases the likelihood of backward bifurcation. Conversely, a larger saturation effect on the recovery rate increases the probability of backward bifurcation.

Numerical simulations were performed to validate the analytical results and explore the impact of varying saturation parameters. We utilized the Mathematical Continuation (MatCont) toolbox within the MATLAB platform to generate bifurcation diagrams for the model under different scenarios. The results illustrate a bistability phenomenon when backward bifurcation occurs, highlighting a complex situation where the long-term solution is heavily dependent on initial conditions. Furthermore, the global sensitivity analysis reveals that the parameters  $u_1$  and  $\delta$  have the most significant influence on changes in the basic reproduction number,  $\mathcal{R}_0$ . This indicates that adjusting either or both of these parameters could significantly alter the value of  $\mathcal{R}_0$ .

**Author Contributions.** Fatahillah, H. A.: Writing – review & editing, Writing – original draft, Visualization, Software, Investigation, Formal analysis. Aldila, D.: Writing – review & editing, Writing – original draft, Supervision, Project administration, Methodology, Investigation, Funding acquisition, Formal analysis, Conceptualization.

**Acknowledgement.** The authors are thankful the editors and reviewers who have supported us in improving the quality of this manuscript.

**Funding.** This research is funded by the Ministry of Research and Higher Education with Fundamental Research Grant Scheme 2024 (ID Number: NKB-894/UN2.RST/HKP.05.00/2024)

**Conflict of interest.** The authors declare no conflict of interest.

**Data availability.** Not applicable.

## References

- [1] H. R. Pandey *et al.*, "Analysis of dengue infection transmission dynamics in nepal using fractional order mathematical modeling," *Chaos, Solitons & Fractals: X*, vol. 11, p. 100098, 2023. DOI:10.1016/j.csfx.2023.100098
- [2] D. Aldila *et al.*, "Unraveling dengue dynamics with data calibration from palu and jakarta: Optimizing active surveillance and fogging interventions," *Chaos, Solitons & Fractals*, vol. 189, p. 115729, 2024. DOI:10.1016/j.chaos.2024.115729
- [3] P. R. Murugadoss *et al.*, "Analysis of dengue transmission dynamic model by stability and hopf bifurcation with two-time delays," *Frontiers in Bioscience-Landmark*, vol. 28, no. 6, 2023. DOI:10.31083/j.fbl2806117
- [4] M. Z. Ndi *et al.*, "Numerical simulations of a two-strain dengue model to investigate the efficacy of the deployment of wolbachia-carrying mosquitoes and vaccination for reducing the incidence of dengue infections," *Journal of Biosafety and Biosecurity*, vol. 6, no. 4, pp. 244–251, 2024. DOI:10.1016/j.jobb.2024.08.003
- [5] A. Raza *et al.*, "Discussion on vector control dengue epidemic model for stability analysis and numerical simulations," *Brazilian Journal of Physics*, vol. 55, no. 1, p. 21, 2025. DOI:10.1007/s13538-024-01656-y
- [6] I. H. Febiriana, A. H. Hassan, and D. Aldila, "Enhancing malaria control strategy: Optimal control and cost-effectiveness analysis on the impact of vector bias on the efficacy of mosquito repellent and hospitalization," *Journal of Applied Mathematics*, vol. 2024, no. 1, p. 9943698, 2024. DOI:10.1155/2024/9943698
- [7] H. Tasman *et al.*, "Assessing the impact of relapse, reinfection and recrudescence on malaria eradication policy: a bifurcation and optimal control analysis," *Tropical Medicine and Infectious Disease*, vol. 7, no. 10, p. 263, 2022. DOI:10.3390/tropicalmed7100263
- [8] B. D. Handari *et al.*, "An optimal control model to understand the potential impact of the new vaccine and transmission-blocking drugs for malaria: A case study in papua and west papua, indonesia," *Vaccines*, vol. 10, no. 8, p. 1174, 2022. DOI:10.3390/vaccines10081174
- [9] J. N. Ndam and P. O. Azike, "Analysis of the transmission dynamics and effects of containment strategies on the eradication of malaria," *Scientific African*, vol. 25, p. e02306, 2024. DOI:10.1016/j.sciaf.2024.e02306
- [10] R. Seck *et al.*, "An age-structured mathematical model for studying malaria transmission dynamics: Applications to some areas of senegal," *Mathematics and Computers in Simulation*, vol. 229, pp. 392–408, 2025. DOI:10.1016/j.matcom.2024.10.006
- [11] C. K. Mahadhika and D. Aldila, "A deterministic transmission model for analytics-driven optimization of covid-19 post-pandemic vaccination and quarantine strategies," *Mathematical Biosciences and Engineering*, vol. 21, no. 4, pp. 4956–4988, 2024. DOI:10.3934/mbe.2024219
- [12] D. Aldila *et al.*, "A mathematical study on the spread of covid-19 considering social distancing and rapid assessment: The case of jakarta, indonesia," *Chaos, Solitons & Fractals*, vol. 139, p. 110042, 2020. DOI:10.1016/j.chaos.2020.110042
- [13] K. Chen *et al.*, "Dynamics of an sveir transmission model with protection awareness and two strains," *Infectious Disease Modelling*, vol. 10, no. 1, pp. 207–228, 2025. DOI:10.1016/j.idm.2024.10.001
- [14] R. I. Gweryina, C. E. Madubueze, and M. A. Nwaokolo, "Mathematical modelling and control of covid-19 transmission in the presence of exposed immigrants," *Communication in Biomathematical Sciences*, vol. 4, no. 2, pp. 93–105 2021. DOI:10.5614/cbms.2021.4.2.2
- [15] M. H. Biswas *et al.*, "Modelling the effect of self-immunity and the impacts of asymptomatic and symptomatic individuals on covid-19 outbreak," *Computer Modeling in Engineering & Sciences*, vol. 125, no. 3, pp. 1033–1060, 2020. DOI:10.32604/cmescs.2020.012792
- [16] A. Din *et al.*, "Mathematical analysis of spread and control of the novel corona virus (covid-19) in china," *Chaos, Solitons and Fractals*, vol. 141, p. 110286, 2020. DOI:10.1016/j.chaos.2020.110286
- [17] G. Simorangkir *et al.*, "Mathematical model of tuberculosis considering observed treatment and vaccination interventions," *Journal of Interdisciplinary Mathematics*, vol. 24, no. 6, pp. 1717–1737, 2021. DOI:10.1080/09720502.2021.1958515
- [18] M. L. Olaosebikan, M. K. Kolawole, and K. A. Bashiru, "Transmission dynamics of tuberculosis model with control strategies," *Jambura Journal of Biomathematics*, vol. 4, no. 2, pp. 110–118, 2023. DOI:10.37905/jjbm.v4i2.21043
- [19] E. D. A. Ginting, D. Aldila, and I. H. Febiriana, "A deterministic compartment model for analyzing tuberculosis dynamics considering vaccination and reinfection," *Healthcare Analytics*, vol. 5, p. 100341, 2024. DOI:10.1016/j.health.2024.100341
- [20] R. K. MA, S. Sugiarto, and S. Nurwijaya, "Dynamical system for tuberculosis

- outbreak with vaccination treatment and different interventions on the burden of drug resistance,” *Jambura Journal of Biomathematics*, vol. 5, no. 1, pp. 10–18, 2024. DOI:10.37905/jjbm.v5i1.21903
- [21] D. Aldila *et al.*, “On the role of early case detection and treatment failure in controlling tuberculosis transmission: A mathematical modeling study,” *Communication in Biomathematical Sciences*, vol. 7, no. 1, pp. 61–86, 2024. DOI:10.5614/cbms.2024.7.1.4
- [22] D. Aldila *et al.*, “Improving tuberculosis control: assessing the value of medical masks and case detection—a multi-country study with cost-effectiveness analysis,” *Royal Society Open Science*, vol. 11, no. 6, 2024. DOI:10.1098/rsos.231715
- [23] D. Aldila *et al.*, “A tuberculosis epidemic model as a proxy for the assessment of the novel m72/as01e vaccine,” *Communications in Non-linear Science and Numerical Simulation*, vol. 120, p. 107162, 2023. DOI:10.1016/j.cnsns.2023.107162
- [24] O. J. Peter *et al.*, “Optimizing tuberculosis control: a comprehensive simulation of integrated interventions using a mathematical model,” *Mathematical Modelling and Numerical Simulation with Applications*, vol. 4, no. 3, pp. 238–255, 2024. DOI:10.53391/mmnsa.1461011
- [25] S. Majee, S. Jana, and T. K. Kar, “Dynamical analysis of monkeypox transmission incorporating optimal vaccination and treatment with cost-effectiveness,” *Chaos*, vol. 33, no. 4, 2023. DOI:10.1063/5.0139157
- [26] I. Smouni *et al.*, “Mathematical modeling and analysis of a monkeypox model,” *Communications in Mathematical Biology and Neuroscience*, vol. 2023, 2023. DOI:10.28919/cmbn/8076
- [27] M. Zevika, A. Triska, and J. W. Puspita, “The dynamics of monkeypox transmission with an optimal vaccination strategy through a mathematical modelling approach,” *Computer Research and Modeling*, vol. 15, no. 6, pp. 1635–1651, 2023. DOI:10.20537/2076-7633-2023-15-6-1635-1651
- [28] A. E. Mansouri *et al.*, “Mathematical modeling and optimal control strategy for the monkeypox epidemic,” *Mathematical Modeling and Computing*, vol. 10, no. 3, pp. 944–955, 2023. DOI:10.23939/mmc2023.03.944
- [29] M. M. Al-Shomrani, S. S. Musa, and A. Yusuf, “Unfolding the transmission dynamics of monkeypox virus: An epidemiological modelling analysis,” *Mathematics*, vol. 11, no. 5, p. 1121, 2023. DOI:10.3390/math11051121
- [30] M. A. Stephano, M. M. Mayengo, and J. I. Irunde, “The role of asymptomatic carriers on the dynamics of a lymphatic filariasis model incorporating control strategies,” *Results in Control and Optimization*, vol. 15, p. 100425, 2024. DOI:10.1016/j.rico.2024.100425
- [31] D. Aldila *et al.*, “Optimal control of pneumonia transmission model with seasonal factor: Learning from jakarta incidence data,” *Heliyon*, vol. 9, no. 7, p. e18096, 2023. DOI:10.1016/j.heliyon.2023.e18096
- [32] M. A. Khan *et al.*, “Dynamic behavior of leptospirosis disease with saturated incidence rate,” *International Journal of Applied and Computational Mathematics*, vol. 2, no. 4, pp. 435–452, 2016. DOI:10.1007/s40819-015-0102-2
- [33] D. Baca-Carrasco, D. Olmos, and I. Barradas, “A mathematical model for human and animal leptospirosis,” in *Journal of Biological Systems*, vol. 23, no. supp01, pp. S55–S65, 2015. DOI:10.1142/S0218339015400057
- [34] G. Zaman *et al.*, “Modeling dynamical interactions between leptospirosis infected vector and human population,” *Applied Mathematical Sciences*, vol. 6, no. 26, pp. 1287–1302, 2012.
- [35] M. A. Khan *et al.*, “Prevention of leptospirosis infected vector and human population by multiple control variables,” *Abstract and Applied Analysis*, vol. 2014, pp. 1–9, 2014. DOI:10.1155/2014/619035
- [36] O. Diekmann, J. A. Heesterbeek, and J. A. Metz, “On the definition and the computation of the basic reproduction ratio  $r_0$  in models for infectious diseases in heterogeneous populations,” *Journal of Mathematical Biology*, vol. 28, no. 4, 1990. DOI:10.1007/BF00178324
- [37] A. B. Gumel, “Causes of backward bifurcations in some epidemiological models,” *Journal of Mathematical Analysis and Applications*, vol. 395, no. 1, pp. 355–365, 2012. DOI:10.1016/j.jmaa.2012.04.077
- [38] O. Sharomi *et al.*, “Mathematical analysis of the transmission dynamics of hiv/tb co-infection in the presence of treatment,” *Mathematical Biosciences and Engineering*, vol. 5, no. 1, pp. 145–174, 2008. DOI:10.3934/mbe.2008.5.145
- [39] A. M. Niger and A. B. Gumel, “Mathematical analysis of the role of repeated exposure on malaria transmission dynamics,” *Dyn. Syst. Differ. Equ.*, vol. 16, no. 3, pp. 251–287, 2008. DOI:10.1007/s12591-008-0015-1
- [40] D. Okuonghae, “Backward bifurcation of an epidemiological model with saturated incidence, isolation and treatment functions,” *Qualitative Theory of Dynamical Systems*, vol. 18, no. 2, pp. 413–440, 2019. DOI:10.1007/s12346-018-0293-0
- [41] O. Diekmann, J. Heesterbeek, and M. G. Roberts, “The construction of next-generation matrices for compartmental epidemic models,” *Journal of The Royal Society*, vol. 7, no. 47, pp. 873–885, 2010. DOI:10.1098/rsif.2009.0386
- [42] C. Castillo-Chavez and B. Song, “Dynamical models of tuberculosis and their applications,” *Mathematical Biosciences and Engineering*, vol. 1, no. 2, pp. 361–404, 2004. DOI:10.3934/mbe.2004.1.361
- [43] S. H. Strogatz, *Nonlinear Dynamics and Chaos: With Applications to Physics, Biology, Chemistry, and Engineering*, CRC Press, Boca Raton, 2018.
- [44] B. P. Statistik, “[metode baru] umur harapan hidup saat lahir (uhh) (tahun), 2022-2024,” 2024, <https://www.bps.go.id/id/statistics-table/2/NDE0IzI=-/metode-baru-umur-harapan-hidup-saat-lahir-uhh.html>, accessed on 28 January 2025.